DOI: 10.1002/ ((smll.201902440))
Article type: Full Paper

A Nature Inspired, Flexible Substrate Strategy for Future Wearable Electronics

*Chuang Zhu, Evelyn Chalmers, Liming Chen, Yuqi Wang, Ben Bin Xu, Yi Li and Xuqing Liu**

C. Zhu, E. Chalmers, Y. Q. Wang, Prof. Y. Li, Dr. X. Q. Liu
School of Materials, University of Manchester, Oxford Road, Manchester, United Kingdom, M13 9PL
E-mail: xuqing.liu@manchester.ac.uk
L. M. Chen
School of Electrical and Electronic Engineering, University of Manchester, Oxford Road, Manchester, United Kingdom, M13 9PL
Dr. B. Xu
Department of Mechanical and Construction Engineering, Northumbria University, Newcastle upon Tyne, United Kingdom, NE1 8ST

Keywords: flexibility, bending sensors, tannic acid, fibers, Kelvin question.

Flexibility plays a vital role in wearable electronics. Repeated bending often leads to the dramatic decrease of conductivity because of the numerous microcracks formed in the metal coating layer, which is undesirable for flexible conductors. Herein, conductive textiles based tactile sensors and metal-coated polyurethane (PU) sponges based bending sensors with superior flexibility for monitoring human touch and arm motions are proposed, respectively. Tannic acid, a traditional mordant, is introduced to attach to various flexible substrates, providing a perfect platform for catalyst absorbing and subsequent electroless deposition (ELD). By understanding the nucleation, growth and structure of electroless metal deposits, the surface morphology of metal nanoparticles can be controlled in nanoscale with simple variation of the plating time. When the electroless plating time is 20 min, the normalized resistance (R/R_0) of our as-made conductive fibers is only 1.6, which is much lower than a 60 min ELD sample at the same conditions ($R/R_0 \approx 5$). This is because a large number of unfilled gaps between nanoparticles prevent metal films from cracking under bending. Importantly, the Kelvin problem is relevant to deposited conductive coatings because metallic

cells have a honeycomb-like structure, which is a rationale to explain the relationships of conductivity and flexibility.

1. Introduction

Recently, there has been rapidly increasing interest in the development of flexible wearable electronics such as tiny motion monitoring sensors,[1-5] wearable energy harvesting and storage devices,[6-13] electronic skins[14] and medical implants.[15-19] The fabrication of flexible conductive materials is one critical step for realizing these devices. Currently, most flexible conductive materials are made by coating metallic layers (Au, Ag, Cu and Ni) on flexible substrates such as textiles,[20-21] polyethylene terephthalate (PET) films,[22-24] poly(dimethylsiloxane) (PDMS),[25-27] sponges[25, 28] and plant leaves.[29-30] Compared with other metal coating candidates, nickel and copper are still considered as the best materials because of their low cost and high electrical conductivity. Many methods of depositing a layer of conductive metals on flexible substrates have been studied, including physical vapor deposition (PVD),[31] chemical vapor deposition (CVD),[32-33] electroplating[34] and electroless deposition (ELD).[35-36] Expensive equipment and complex operation steps are required for PVD and CVD. Electroplating needs the conductive substrate to activate the metal deposition, which is not suitable for the major of polymeric substrates. In general, ELD is particularly attractive for the metallization of flexible surfaces because it can be conducted under ambient conditions on a large scale without the requirement of expensive equipment.

Notably, pretreatment of substrates is crucial in ELD. Polymer-assisted metal deposition (PAMD) is a full-solution processing strategy, in which the surface-grafted polymer is innovatively introduced to facilitate the ELD on polymer substrates. The polymer interface molecular engineering plays an important role in PAMD because the grafted polymer acts as an adhesion layer for the deposited metal film and improves the uptake efficiency and selectivity of the catalyst.[37] Several polymer interfaces, including poly[2-(methacryloyloxy)-

ethyltrimethlammonium chloride] (PMETAC)[38] and polydopamine (PDA),[39-40] have been reported in previous works. Although highly flexible and durable conductors are manufactured via ELD assisted by PMETAC, there are still some drawbacks existing in this method. The synthesis of PMETAC is very complex and the surface-grafting technique of PMETAC requires N_2 protection. Additionally, plasma treatment is required when the target substrates do not contain abundant hydroxyl groups. In contrast to PMETAC, dopamine, a kind of biomaterial found in mussels, provides a promising opportunity by allowing the self-deposition of adherent PDA films on virtually all material surfaces via simple dip coating in an alkaline solution without any pretreatment.[41] More importantly, catalysts can be anchored by PDA interfaces for subsequent ELD.[42] Therefore, such a phenol-rich material seems like an ideal alternative candidate for PMETAC-assisted metal deposition. Nevertheless, dopamine is expensive and the PDA modification process is time-consuming (24 h), which are less favoured for industrial production.

To address this need, we here report a facile, low-cost and universal method for fabricating high-performance compliant flexible conductive composites at industrial scales. The key-enabling feature of this strategy is the introduction of tannic acid (TA) as the designed interface via dip coating and subsequent catalyst-activated ELD. Inspired by textile dyeing and coloration processes, TA can form mordant combinations (TA + metal salts) on the fiber surface through the interaction of the TA anions and metal cations such as Fe^{3+}, indicating the metal ion chelating/reducing ability of TA.[43] Compared with PDA, TA is abundant in many plants such as gallnuts and the price of TA is relatively hundredfold lower than that of dopamine. Moreover, the time taken for the TA coating on almost all inorganic and organic surfaces is significantly shortened. Importantly, the TA aqueous solution is air stable and can be stored in the laboratory for more than one month. As proofs-of-concept applications, as-prepared conductive yarns and fabrics are demonstrated as conductors to power the light-emitting diode (LED) in a simple circuit. This approach is compatible with typical surface

lithography techniques (e.g., screen printing) for making desired conductive patterns. In addition, durable bending sensors based on Ni-coated PU sponges obtained via ELD are used to detect arm motions. Interestingly, we found that there is an intrinsic link between conductivity and flexibility in flexible conductors created by solution deposition techniques. This intrinsic link is explained by the Kelvin Problem model in metallic grain growth and will be scientific law in the design of future flexible devices.

2. Results and Discussion

2.1. Surface Chemical Characterization

The fabrication of metal-coated flexible and stretchable conductors consists of TA coating, catalyst immobilization and ELD, as illustrated in **Figure 1**. In brief, TA was first attached to flexible surfaces via intermolecular hydrogen bonds by immersing these cleaned substrates into the TA aqueous solution. Such a polymerized plant-based phenolic coating offers sufficient sites to anchor catalysts for subsequent ELD. Pyrogallol-rich solutions such as red wine, coffee and red tea were also able to successfully coat pyrogallol moieties on flexible surfaces, immobilize catalysts, and then activate ELD.[44]

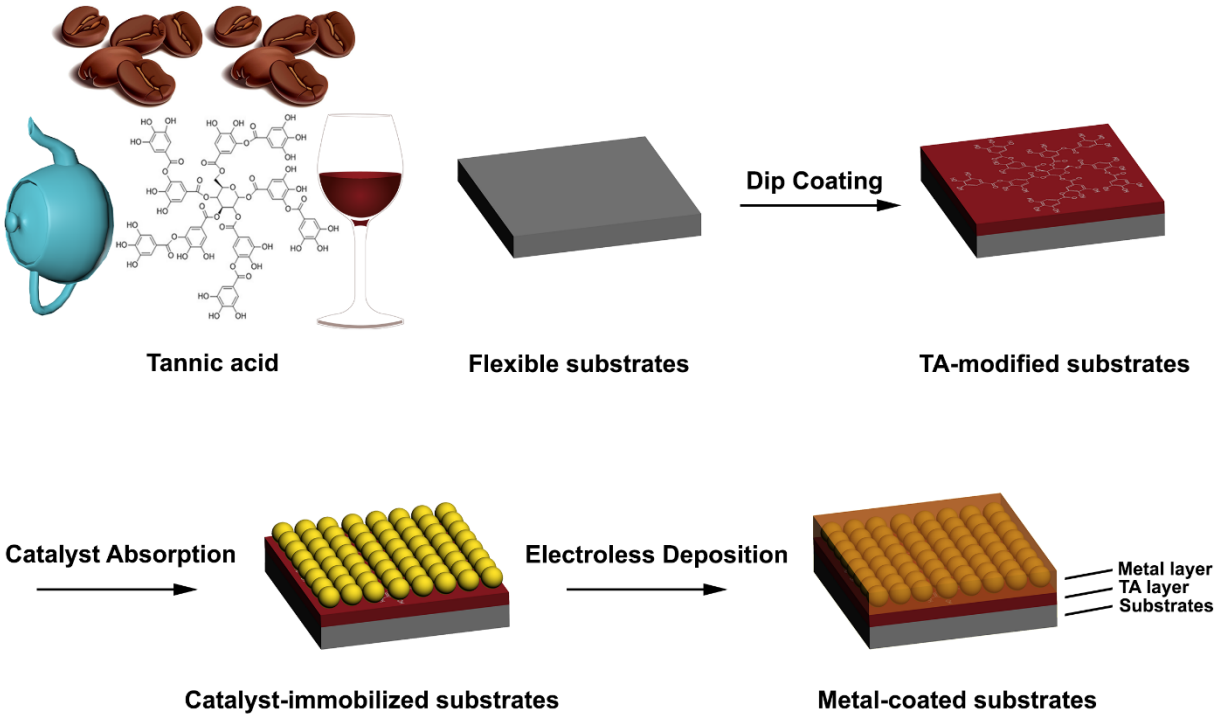

Figure 1. The scheme illustration for the fabrication of flexible conductors via TA modification and electroless deposition.

Fourier transform infrared spectroscopy (FTIR) was used to confirm the coating of TA. Pristine and TA-modified cotton fabrics were compared because of cotton's wide use in daily life. From **Figure 2**a, the new peak at around 1715 cm^{-1} is assigned to the C=O stretching of carbonyl groups in TA. The medium intensity band at 1605 cm^{-1} is associated with the C=C stretching vibration of aromatic groups in TA. The raw polyurethane (PU) sponge and TA-coated PU sponge were analyzed due to its unique three-dimensional and hollow structure. From Figure 2b, the strengthened peak at 3270 cm^{-1} is attributed to the O-H strecthing state of phenol groups in TA. After the TA modification, the TA-modified substrates were dipped into a 5mM $(NH_4)_2PdCI_4$ aqueous solution for 15 min to anchor catalysts. The binding mechanism between TA and Pd (II) is very important in this catalytic system and will affect the catalytic performance. Therefore, X-ray photoelectron spectroscopy was used to characterize the surface chemical composition in the Pd/TA-PET film. The proposed binding

mechanism between TA and palladium ions is shown in Figure 2c. From Figure 2d, two spin-orbital doublets are shown in the Pd 3d spectrum, indicating two electronic states of palladium in the catalytic surface.[45] The peaks at 337.6 eV and 347.4 eV are attributed to Pd (0) species and the peaks at 342.8 eV and 351.0 eV are assigned to Pd (II) species. However, these reduced Pd nanoparticles do not exhibit significant catalytic behaviour because when extra reductants were added to reduce more Pd ions into Pd nanoparticles on the surface of TA-PET, the sample would not activate the ELD. Thus, chelated Pd ions in TA by phenol groups were the major cause that initiated the ELD. To investigate the effect of TA on binding catalysts, a raw PET film without any surface modification was immersed into the same seeding solution. The XPS results of the Pd-PET film show that the peaks in the Pd 3d signal spectrum have the same binding energy but the intensity of these peaks is much lower than that of the Pd/TA-PET film (Figure S1, Supporting Information). The Pd (0) and Pd (II) species in the Pd-PET sample might be anchored by cation-π interaction[46] between benzene groups in PET and Pd ions. Therefore, it can be clearly seen that phenol groups in TA play an important role as a binder to anchor catalysts.

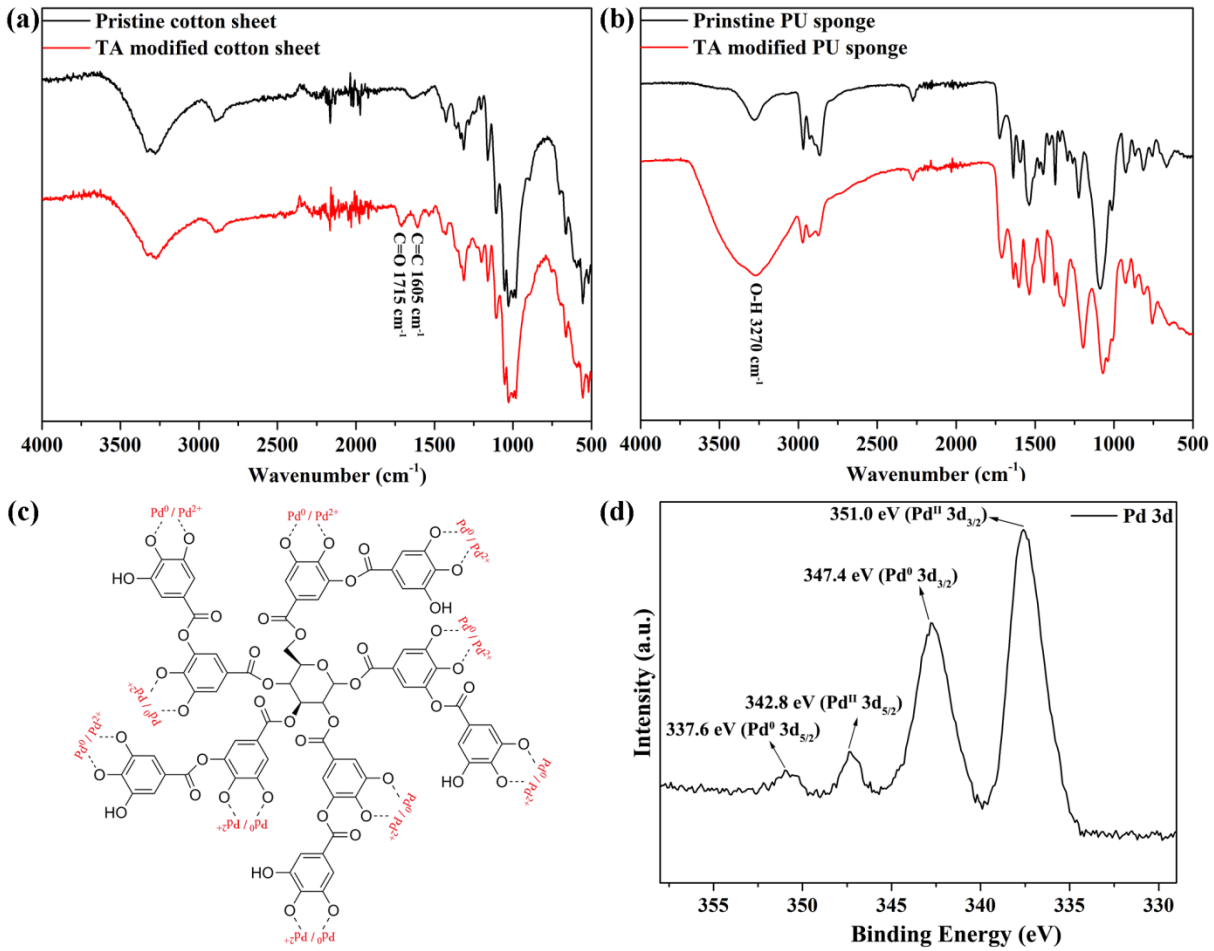

Figure 2. The transmittance FTIR spectrum of a) The cotton fabric and b) The PU sponge, without any modification (black) and with TA coating (red). c) The proposed binding mechanism between TA and Pd ions and d) The XPS spectrum of Pd 3d for the Pd/TA-PET film.

2.2. Surface Morphology Characterization

The electrical, mechanical and optical properties of as-made conductive samples may be affected by the surface morphology of the deposited metal nanoparticles. Scanning electron microscopy (SEM) was thus employed to explore the morphology of the obtained metal coating. Fiber assemblies and sponges will cause a decrease in uniformity and continuity of metal films deposited by gravity-initiated methods such as sputtering. This is because yarns and fabrics have the unique porous structure and PU sponges contain the particular 3D framework. For this reason, metal-coated cotton fibers and sponges, manufactured by our

method, are discussed in the SEM characterization. The SEM photographs of pure cotton fibers (a), the untreated sponge (b), Ni-coated cotton fibers (c) and the nickel coating on the PU sponge (d) are shown in **Figure 3**. It can be clearly seen that the surface morphology of unmodified materials changed significantly after Ni ELD. As shown in Figure 3c,d, Ni nanoparticles were very homogeneously, continuously and densely covered on the surface of these two substrates. The electrical performance of the as-prepared flexible conductors would be enhanced by the compact and uniform nickel nanoparticle film. More importantly, the coating layer is fully deposited on the multidirectional surfaces. In other words, homogenous and continuous nickel nanoparticles were compactly dispersed on both of the outer and inner layer of the substrates. This would also enhance the electrical properties of the as-made metallic flexible substrates. After Cu ELD, the surface of PET fiber substrates is also fully packed with dense aggregates of Cu nanoparticles (Figure S2, Supporting Information). The crystalline structure and size of nickel and copper nanoparticles deposited on flexible samples were detected by X-ray diffraction (XRD). From Figure 3e, nickel-coated samples show a characteristic peak at the 2θ value of 44.9^0. According to the standard power diffraction card of Joint Committee on Powder Diffraction Standards (JCPDS), this peak is associated with the (111) crystal face of face-centered cubic (fcc) Ni (JCPDS no. 45-1027). The average size of the crystalline metallic Ni nanoparticles was c.a. 16.5 nm according to the Scherrer equation. The obtained data from XRD is coincident with the above-listed SEM results, in which the ELD time is 20 min. Figure 3f shows that the big clusters (300-500 nm) are made of numerous small nanoparticles (15-20 nm) when the ELD time is 60 min. This proves that Ni nanoparticles are deposited on samples with the same size throughout the whole ELD process. The XRD spectrum of Cu-coated samples shows three main peaks at 2θ values 43.9^0, 51.0^0 and 74.7^0 corresponded to the (111), (200) and (220) planes, respectively, with the Cu nanoparticles also maintaining the same size during the ELD (Figure S3, Supporting Information). The average size of copper particles (the crystal plane is 111) was c.a. 31.1 nm.

We found that the Cu-deposited samples suffered a decrease of electrical conductivity after exposing them to air for 7 days. This is due to the oxidation of copper nanoparticles in air and it may be addressed by capping the metal by some developed methods in the electronic industry such as physical encapsulation.

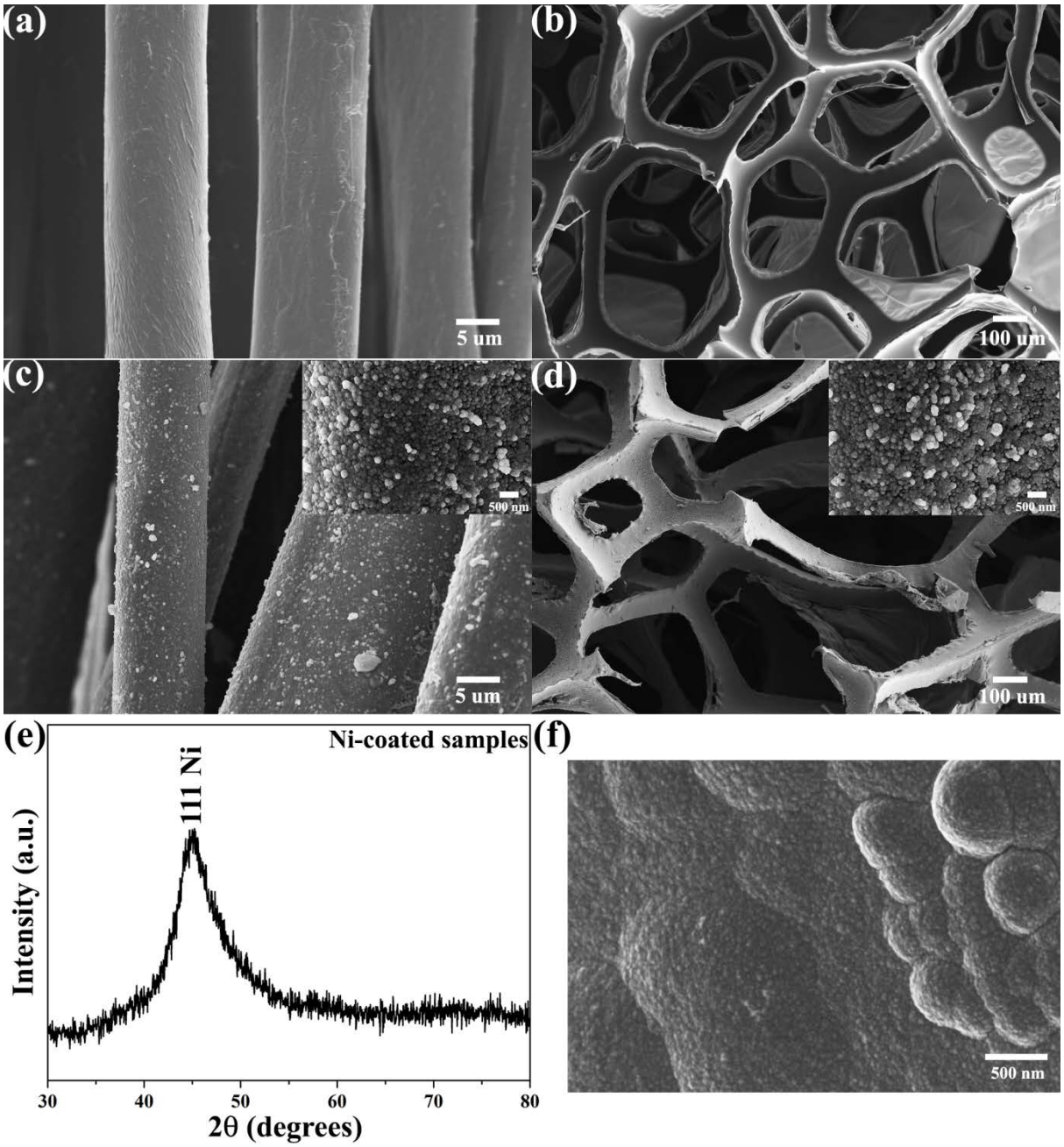

Figure 3. SEM photographs of cotton fibers and the PU sponge a,b) Without any treatment and c,d) With the nickel coating (20 min ELD). Insets are magnified images. e) The XRD

spectrum of Ni-deposited flexible substrates and f) The SEM photograph of Ni-coated samples (60 min ELD).

2.3. Electrical Conductivity, Flexibility and Mechanical Durability

It is well-known that bare polymers are electrically insulating at room condition. In contrast, Ni-coated polymeric substrates prepared by our method are electrically conductive. In this report, highly conductive Ni films were homogeneously coated on sheets of cotton, wool, nylon fabric, PET films, PU sponges, and natural luffa sponges (Figure S4, Supporting Information). Surprisingly, the resistance of the single aramid fiber coated by copper can reach as low as 0.9 Ω/cm. And Our results showed that the hydrophilic substrates containing amine groups can achieve higher conductivity due to more TA bonding on the substrates.[44] However, we found that the metal coating on amine-rich substrates such as wool is not very good, leading to lower conductivity. The reason might be that phenolic hydroxyl groups of TA molecules functionalize with protein molecules in wool to form complexes,[47] resulting in the decreased number of phenol groups available to immobilize catalysts. Thus, the formation of complexes between protein and TA would adversely affect the catalyst immobilization and subsequent ELD. From previous reports, the conductivity of metal-coated substrates increased with extending the ELD time.[48] However, limited reports discussed the flexibility of metal-coated samples during the ELD process in their intrinsic principle. Thus, British Standard (BS) 3356:1990, which is a method for determination of bending length and flexural rigidity of fabrics, and a two-point probe method, were applied to test the bending length in warp direction and the surface resistance of Ni-coated cotton fabrics in different ELD times, respectively. From **Figure 4**a, it is clear to see that longer ELD leads to decreased surface resistance but increased bending length. After 10 min of plating, the surface resistance and the warp-wise bending length of Ni-coated fabric is 3230 Ω/sq and 1.925cm, respectively. Such a low value of the bending length indicates that this sample was very flexible. From Figure 4g,

it can be seen that nickel nanoparticles were not fully covered on the fiber surface, indicating the excellent flexibility and the poor conductivity of the 10 min ELD sample. Thus, as shown in Figure 4c, when 1000 mechanical bending cycles (bending radius = 0.1 mm) were applied in the 10 min ELD sample, there was no obvious change in the surface resistance ($R/R_0 \approx 1.1$). After 20 min of depositing, a quick decrease of surface resistance (16.68 Ω/sq) can be observed and the bending length in warp direction of our as-prepared fabric is 2.325 cm. The increased value of bending length demonstrates that this sample was less flexible than the 10 min ELD sample. From Figure 4h, although nickel nanoparticles were fully packed on the fiber surface with a multilayers-shaped structure, there were numerous gaps between these building blocks. These unfilled gaps could prevent the nickel films of the 20 min ELD sample from cracking under large bending, as illustrated in Figure 4b. Therefore, only a small increase of surface resistance ($R/R_0 \approx 1.6$) in the mechanical bending test was illustrated in Figure 4d. With a longer plating time (30 min), the surface resistance and the warp-wise bending length of Ni-deposited sample is 5.29 Ω/sq and 2.725 cm, respectively. The slow decrease rate of surface resistance was due to catalyst poisoning. The value of bending length increased continuously, indicating the stiffer Ni-coated fabric. From Figure 4i, nickel nanoparticles aggregated to form clusters on the surface of the coating layer, resulting in the brittle and stiff nickel film. As a consequence, the 30 min ELD sample showed a quick increase of the normalized resistance in the bending test from 1 to 3 in Figure 4e. After 60 min of electroless plating, the surface resistance showed a small decrease from 5.29 to 1.02 Ω/sq, which is due to the further catalyst deactivation. However, the value of the bending length in warp direction experienced a large increase from 2.725 to 3.925 cm, demonstrating higher stiffness of as-made samples. From Figure 4j, nickel nanoparticles continued to aggregate and form bigger and more compact clusters, causing a more brittle and stiff nickel film. The particle aggregation significantly increased the value of bending length but had a very limited impact on surface resistance. From Figure 4f, the 60 min ELD sample illustrated

a dramatic increase of the normalized resistance in the mechanical bending cycles from 1 to 5, which is ascribed to the very low flexibility of the nickel-coated sample. After the bending test, the obvious cracking could be found in the nickel coating layer of the 60 min ELD fabric (Figure S5, Supporting Information). Hence, based on the above discussion, the optimized ELD time of Ni metallization for manufacturing flexible conductive fibers was 20 min and the nickel film exhibited the multi-layer structure with a great number of unfilled gaps between nickel nanoparticles. Additionally, the deposition of the Ni coating on flexible substrates includes three stages: (i) the nucleation period (loose coating, highest flexibility), (ii) the growth of spherical nodules period (the multi-layers shape, medium flexibility), (iii) the aggregating of nanoparticles period (clusters, lowest flexibility) (Movie S1, Supporting Information) and the surface morphology of metal deposits can be controlled in nanoscale by varying ELD time. The cooper-coated samples showed the same growth process (Figure S6, Supporting Information) and we found that metal aggregates in the outer surface of the coating layer are bigger than particles in the inner surface of the metal coating layer (Figure S7, Supporting Information).

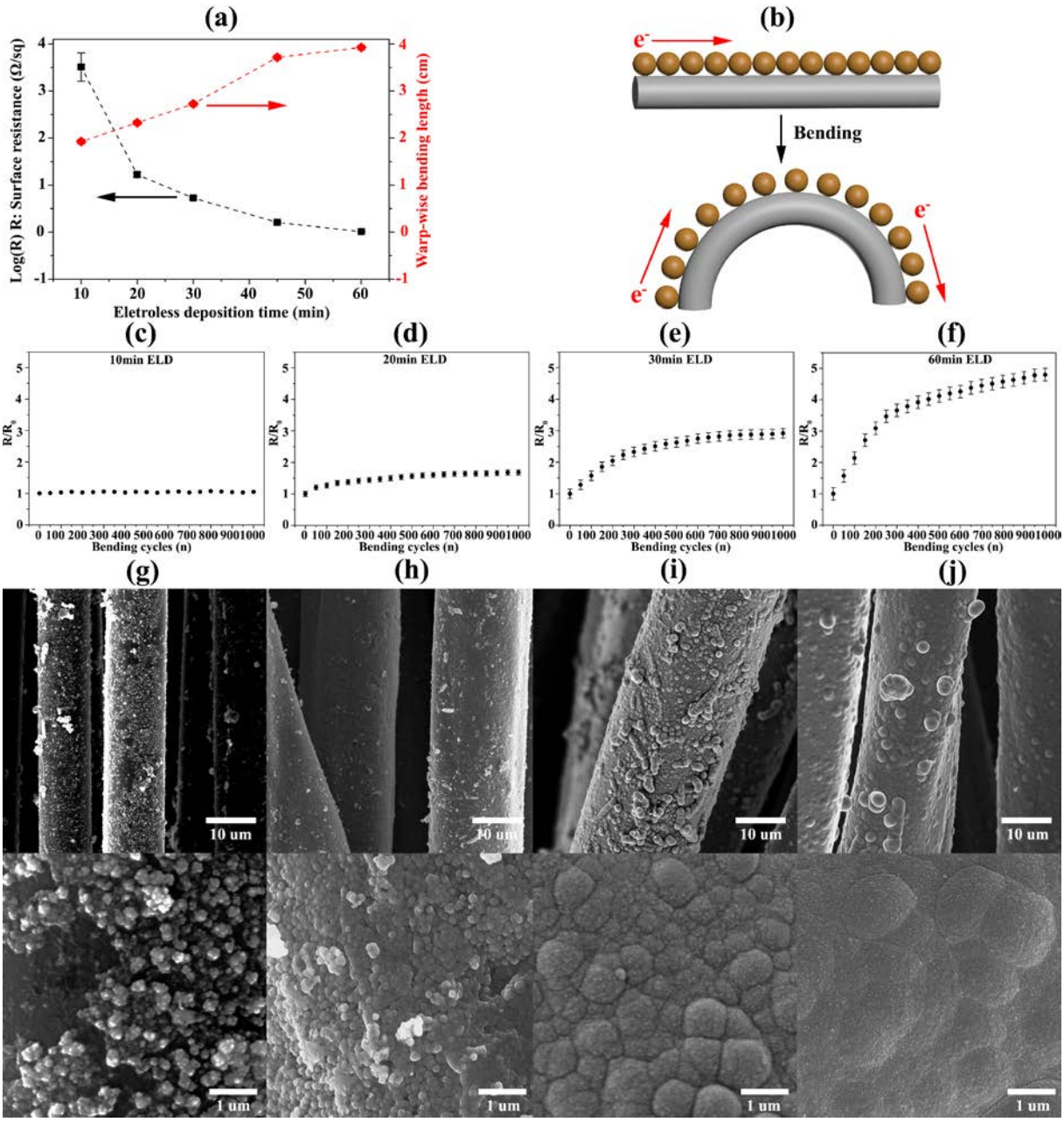

Figure 4. a) The Surface resistance (squares) and the bending length in warp direction (diamonds) of Ni-coated cotton fabrics obtained at different ELD times. b) The scheme illustration of electrons conducting in the inner conductive layer of metal-coated fibers during releasing and bending. The bending cycles (r = 0.1 mm) versus the normalized resistance when the nickel-coated sample is at c) 10 min ELD, d) 20 min ELD, e) 30 min ELD and f) 60 min ELD. The SEM images of Ni-coated cotton fabrics when the fabric is at g) 10 min ELD, h) 20 min ELD, i) 30 min ELD and j) 60 min ELD.

2.4. Kelvin Structure Model

To further explore the relationship between conductivity and flexibility of surface deposited metallic coating on flexible substrates, we introduce the Kelvin Structure model to understand this intrinsic connection. The Kelvin problem, posed by Lord Kelvin in 1887, to find space-filling arrangement of similar cells, of equal volume, is relevant to deposited conductive coatings in this research because deposited metallic cells have a honeycomb-like structure. Under the observation of SEM (a,c), the morphologies of deposited layers (20 min ELD and 60 min ELD) are similar to the arrangement of bubble foams (b,d), as shown in **Figure 5**. At the beginning of the deposition, the clusters are isolated, so that the conductivity of coating is poor but shows excellent flexibility, due to less attachment of each isolated particle. During the increased deposition time, if the plating solution keeps a constant concentration, ideally, as a self-catalysing reaction, the metallic clusters will undergo competitive growth and squeeze with neighbour clusters, to form honeycomb-like structure by minimizing energy, following the Aboav–Weaire empirical topological law.[49] Similar to coarsening in soap films, the size of metallic clusters grows due to pressure differences between cells, which follows the Von Neumann's Law well. Neighbour swapping and bubble disappearance are two primary reasons in topological changes in metallic coating deposition, by reducing perimeter (Figure S8 Supporting Information).[50] From the observation of the cross section of coating, the SEM image in Figure 5e shows that on the bottom of the coating, the clusters are small and incompact. However, the clusters on the top of the coating, during the coarsening process, are bigger and more compact, as shown in Figure 5f. During bending, the surface stress released from the top surface of films to the incompact bottom, is smaller compared with homogeneous structures, such as copper foil. An opposite example is the metal block material. After repeated bending, there will be some defects in the metal block material, to release the stress from the bending. As the defects continue to grow and spread, it can cause material breakage.[51] This is the main reason why the ductility of the ductile metal film produced by

the physical method is not high. Thus, this hierarchical structure makes the conductive fibers or films show both excellent conductivity and flexibility. Introducing the Kelvin Structure model allows improvement in predicting the flexible and conductive properties of the chemical deposited coating, in both ELD and electrodeposition.

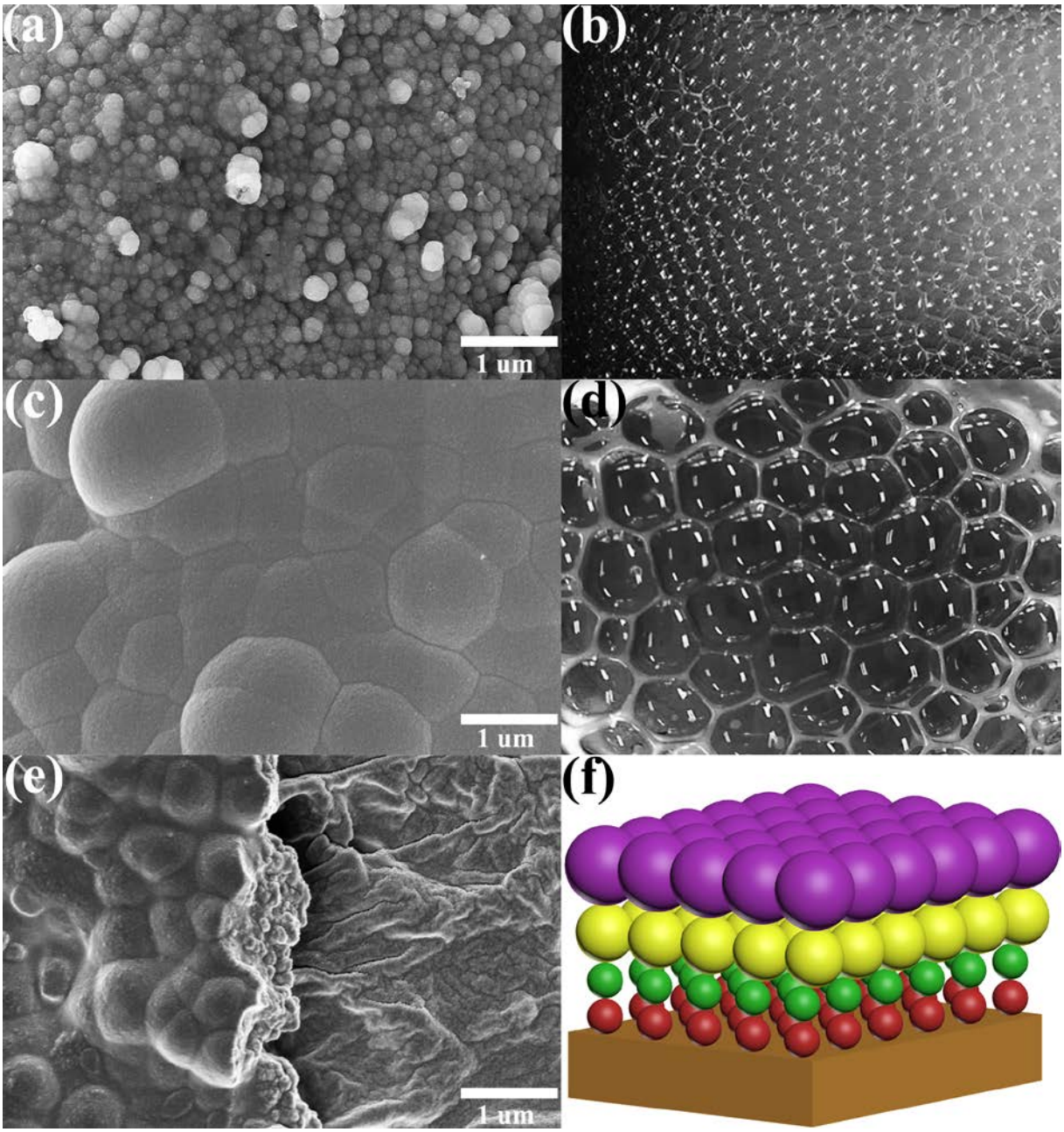

Figure 5. a) The SEM image of the morphologies of deposited layers at 20 min ELD. b) The arrangement of small bubble foams. c) The SEM photograph of the plated particles at 60 min

ELD. d) The arrangement of big bubble foams. e) The SEM image of the cross section of coatings. f) The scheme illustration of the size of particles in different layers.

2.5. Practical Demonstrations

As this chemical strategy is a universal nature-inspired method for metallizing virtually all material surfaces, it can be readily extended to making metal-coated conductive fibers, yarns and fabrics. The most important application of as-made conductive textiles is demonstrated as conductive wires and substrates in integrated electronic circuits due to their excellent electrical conductivity and high robustness. For proof-of-concept purposes, we built a simple circuit by connecting a 9 V alkaline battery with one electrical contact of a red LED with manufactured Ni-coated nylon yarns and Cu-plated cotton fabrics. When the battery contacted to the other contact of LED, the LED switched on immediately and illuminated for more than 10 min until the disconnection of contact was made (Figure S9, Supporting Information). Notably, this method shows excellent compatibility with screen printing for preparing desired conductive patterns. As shown in **Figure 6**a, there are two strategies to fabricate well-defined metal conductive patterns onto flexible polymeric substrates via screen printing. In strategy A, the substrate is firstly coated with TA, which plays a role of the receiving matrix polymer. Catalytic salt is then screen printed with the help of polyethylene glycol (PEG), functioning as the delivering matrix polymer, onto the TA-modified substrate. After printing, catalyst patterns are formed on the substrate with a thin layer of TA because the inorganic catalytic salts diffuse from the PEG into TA upon the contact between the two matrix polymers. Metal patterns are finally manufactured by electroless plating on the catalytic area. While in strategy B, TA is initially screen printed with the aid of the PEG onto the raw substrate to form TA patterns. The substrate partially modified by TA is subsequently immersed into the aqueous solution containing catalytic salts and catalytic patterns are formed on the ink-patterned area because only TA-modified area can capture catalysts. ELD is finally conducted on the

catalyst-immobilized area to fabricate metal patterns on flexible substrates. Printing gels were prepared by mixing PEG, TA, $(NH_4)_2PdCI_4$ and DI water in different ratios (Table S1, Supporting Information). Compared with normal polymer substrates, textiles endowed with conductive properties provide a more powerful platform for wearable electronics because they are lightweight and skin-friendly.[52] Thus, metal patterns are fabricated on textile substrates in this report. As presented in Figure 6b, the Ni interdigital electrode is fabricated onto the flexible cotton fabric via screen printing. Additionally, the SEM image of the Ni pattern obtained through ELD on the cotton fabric shows a clear boundary, as shown in Figure 6c. This indicates that the well-defined nickel pattern was fabricated using our strategy. Furthermore, to demonstrate potential applications of the proposed manufacturing route in wearable electronics, a simple circuit with our as-made conductive yarns and one conductive keypad was built for controlling the red LED light via human touch, as shown in Figure 6d. From Figure 6e, when the keypad was connected by the human finger, the red LED was illuminated. This phenomenon shows that the fabricated metal pattern can play the role of a stable conductor on textile substrates for practical use.

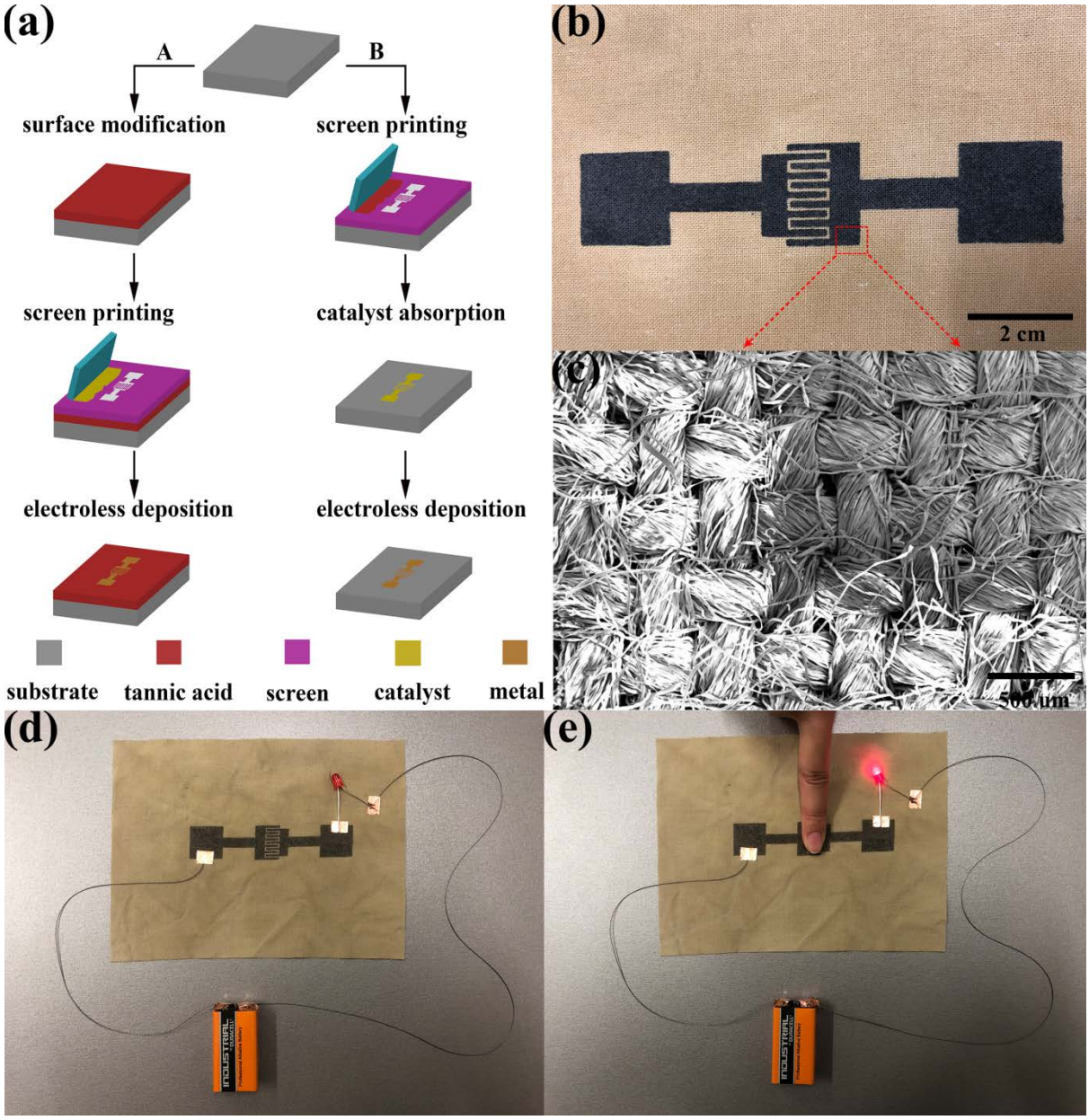

Figure 6. a) The scheme illustration of the manufacturing of conductive patterns via screen printing. b) The digital photograph of the cotton fabric with screen-printed conductive interdigital electrode. c) The SEM photograph of the clear boundary between the cotton fabric and the Ni pattern. d) The designed simple circuit for controlling the LED light via human touch. e) The LED was lit when the keypad was connected.

More importantly, when applying our approach to a piece of PU sponge, several Ni-metallized PU sponges with different flexibility and conductivity can be obtained. As shown

in **Figure 7**a, different weights from 0 to 100 g were placed on the top of the Ni-coated sponge, respectively. This would cause the change of resistance signal, which can be detected by the Keithley 2000 Multimeter. On the basis of the above study, 10 min ELD and 20 min ELD samples are very flexible and further extending ELD time leads to rigid and brittle samples. From Figure 7b,c, when the weight increased from 0 to 5 g, there was no obvious change in the surface resistance of 10 min ELD and 20 min ELD Ni-plated sponges. When the weight further increased, this would induce increasing pressure and cause more contact area in the 3D structure, increasing the conductive pathway.[53] As a result, the resistance signal would decrease accordingly. When the weight was removed, the resistance recovered to its original value due to the reestablishment of the conductive network. The responses of the resistance signal are similar when repeating loading/removing of the weight because the high flexibility of these two Ni-coated sponges can prevent cracking under large deformation. As shown in Figure 7d,e, when the weight increased from 0 to 5 to 20 g, the surface resistance of 30 min ELD and 60 min ELD samples showed a small increase because the loaded pressure induced crack propagation in the brittle and stiff Ni film and the micro/nano cracks decreased the number of conductive pathways.[54-55] When the weight further increased, although large and rapid crack propagation was promoted, more contact area occurred between sponge scaffolds, enabling dramatic increase of the conductive pathway and thus, the surface resistance decreased. However, when the 100 g weight was removed, the surface resistance experienced a significant increase because of the numerous irreversible cracking (Figure S10, Supporting Information) and the reduction of contact area, resulting in the loss of conductivity. More importantly, these two samples could not detect the tiny pressure after one cycle because the well-coated nickel film was destroyed. Thus, when the 5 g weight was placed on the top of these two samples again, no obvious change of resistance could be detected. When further increasing the weight, the resistance signal is similar to the 10 min and 20 min ELD samples. Only two cycles are shown in this test because the inherent flexibility of sponges is

much lower than that of textiles and more cycles would lead to the resistance of 30 min ELD and 60 min ELD samples changing from low to infinity. To further investigate the ability of this resistance sensor in monitoring bending movements of the human arms, the 20 min ELD Ni-coated PU sponge, which was considered as the best ELD time for cracking-control conductive PU sponges, was attached to the arm part of the human body, as shown in Figure 7f. From Figure 7g, the resistance of the attached conductive sponge decreased during bending arms and the resistance signal showed a quick increase during releasing arms. This was because the bending/releasing induced more/less strain in the hollow structure, increasing/decreasing the contact area between Ni coatings. Repetition of the arm movements leads to similar resistance responses for each cycle because the 20 min ELD Ni-coated PU sponge is very durable.

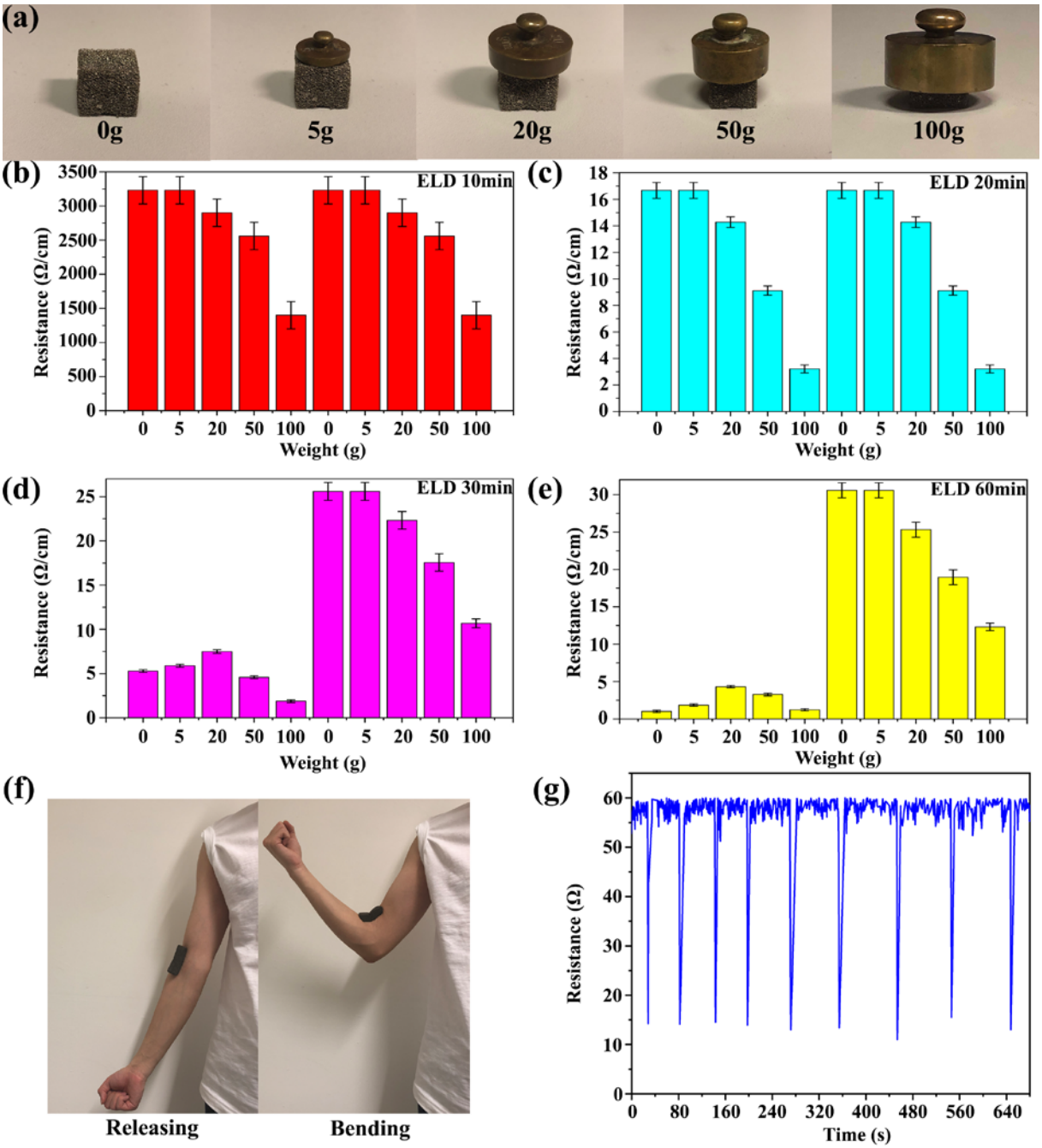

Figure 7. a) The digital images of different weights on the top of the Ni-coated PU sponge. The weight versus resistance when the nickel-coated PU sponge is at b) 10 min ELD, c) 20 min ELD, d) 30 min ELD and e) 60 min ELD. f) The digital images of the Ni-coated PU sponge attached on the human arms. g) The change of resistance for the attached Ni-coated sponge with human arms bending.

3. Conclusion

In conclusion, a novel, facile and universal strategy of preparing conductive flexible substrates by TA modification and electroless plating of metal with strong adhesion is introduced. The key innovation of this method is the use of TA as a solid bridge between all demonstrated surfaces and Pd^{2+} seeds, capturing Pd^{2+} and partially reducing Pd^{2+} into Pd nanoparticles. Subsequently, the site-selective ELD can be performed to yield high-quality metal coatings for flexible electronics at room temperature. This versatile approach has several unique advantages in the following aspects. Firstly, the naturally abundant TA is very cheap and the TA modification solution can be reused for more than one month, holding great promises for large-scale production in the industry. Secondly, TA can covalently tether one end on virtually all material surfaces with strong adhesion, which is favorable for the assembly of flexible conductors. Thirdly, this strategy shows superior compatibility with screen printing on textile substrates, offering great potential for the high-throughput fabrication of wearable electronics. Fourthly, by understanding the mechanism of electroless plating with the aid of SEM, the cracking control can be achieved by varying ELD time to produce highly stretchable conductors and the high conductivity can be maintained after repeated stretching. Therefore, such a novel method can be anticipated to inspire remarkable applications in fields of robotic skins, fiber-shaped wearable devices, biomedical industries, etc. Lastly, in order to explore in depth, the relationship between conductivity and flexibility of surface deposited metallic coating on flexible substrates, we introduce the Kelvin Structure model to understand the mechanism of clusters growth, and to optimize conductivity and flexibility.

4. Experimental Section

Materials: Tannic acid, ammonium tetrachloropalladate (II) [$(NH_4)_2PdCI_4$] and all other chemicals were purchased from Sigma-Aldrich. All flexible substrates were provided by the

Dye House at the University of Manchester. All chemicals were used without further purification. Each substrate was ultrasonically cleaned in acetone and deionized (DI) water for 30 min, respectively and dried with a N_2 gas stream.

Polymer Interface Molecular Engineering: Tannic acid was dissolved in DI water to prepare a tannic acid aqueous solution (5 g/L). After dipping cleaned substrates into the solution for 30min, the tannic acid coated surfaces were rinsed with DI water several times and then dried under a stream of N_2.

Electroless deposition: catalysts were immobilized by immersing the modified samples into a 5mM $(NH_4)_2PdCI_4$ aqueous solution and placed in a dark environment for 15 min. The physical absorption of catalysts was removed by thorough rinsing with DI water. The Ni electroless plating was performed in an ELD bath containing 4:1 mixture of freshly prepared solutions A and B at room temperature. Solution A consisted of 10 g/L lactic acid, 20 g/L sodium citrate and 40 g/L nickel sulfate hexahydrate prepared in advance. Solution B was a freshly prepared reductant solution containing 1 g/L dimethylamine borane (DMAB) in DI water. After mixing, the solution was adjusted with ammonia to pH ~8. The Cu electroless deposition was performed in plating bath containing 1:1 volumetric proportion of nickel-to-reductant stocks at room temperature. A copper stock solution consisting of 12 g/L NaOH, 13 g/L $CuSO_4 \cdot 5H_2O$ and 29 g/L $KNaC_4H_4O_6 \cdot 4H_2O$ was prepared in advance. A fresh reductant solution containing 9.5 mL/L HCHO in DI water was prepared separately. After ELD, all samples were washed several times and dried with compressed air.

Characterization: The coating of tannic acid on flexible substrates was tested by Fourier transform infrared spectroscopy (NICOLET 5700 FTIR). The surface composition of catalyst-anchored substrates was analyzed by XPS Near Ambient Pressure. The surface morphology of the samples was investigated by scanning electron microscopy (ZEISS Ultra-55 and TESCAN LC Mira3). The size and the shape of the unit cell for metallic particles on the sample surface were characterized by X-ray diffraction (PANalytical X'Pert Pro X'Celerator diffractometer).

A 2-point probe method with a Keithley 2000 Multimeter was used to measure the resistance of flexible surfaces.

Supporting Information
Supporting Information is available from the Wiley Online Library or from the author.

Acknowledgements
The Authors thank Dr. Ben Spencer from University of Manchester on the assistance of XPS characterization.

Received: ((will be filled in by the editorial staff))
Revised: ((will be filled in by the editorial staff))
Published online: ((will be filled in by the editorial staff))

References

[1] X. Wu, Y. Han, X. Zhang, C. Lu, *ACS Appl. Mater. Interfaces* **2016**, 8, 9936.
[2] W. A. D. M. Jayathilaka, K. Qi, Y. Qin, A. Chinnappan, W. Serrano-García, C. Baskar, H. Wang, J. He, S. Cui, S. W. Thomas, S. Ramakrishna, *Adv. Mater.* **2019**, 31, 1805921.
[3] S. Seyedin, P. Zhang, M. Naebe, S. Qin, J. Chen, X. Wang, J. M. J. M. H. Razal, *Mater. Horiz.* **2019**, 6, 219.
[4] Q. Liu, J. Chen, Y. Li, G. Shi, *ACS Nano* **2016**, 10, 7901.
[5] J. S. Heo, J. Eom, Y.-H. Kim, S. K. Park, *Small* **2018**, 14, 1703034.
[6] J. Bae, Y. J. Park, M. Lee, S. N. Cha, Y. J. Choi, C. S. Lee, J. M. Kim, Z. L. Wang, *Adv. Mater.* **2011**, 23, 3446.
[7] Z. Yang, J. Deng, X. Sun, H. Li, H. Peng, *Adv. Mater.* **2014**, 26, 2643.
[8] M. R. Lee, R. D. Eckert, K. Forberich, G. Dennler, C. J. Brabec, R. A. Gaudiana, *Science* **2009**, 324, 232.
[9] D. Yu, K. Goh, H. Wang, L. Wei, W. Jiang, Q. Zhang, L. Dai, Y. Chen, *Nat. Nanotechnol.* **2014**, 9, 555.
[10] R. Dong, Q. Ye, L. Kuang, X. Lu, Y. Zhang, X. Zhang, G. Tan, Y. Wen, F. Wang, *ACS Appl. Mater. Interfaces* **2013**, 5, 9508.
[11] X. Zheng, H. Quan, X. Li, H. He, Q. Ye, X. Xu, F. Wang, *Nanoscale* **2016**, 8, 17055.
[12] Q. Ye, R. Dong, Z. Xia, G. Chen, H. Wang, G. Tan, L. Jiang, F. Wang, *Electrochim. Acta* **2014**, 141, 286.
[13] L. Li, Z. Lou, D. Chen, K. Jiang, W. Han, G. Shen, *Small* **2018**, 14, 1702829.
[14] G. Schwartz, B. C. K. Tee, J. Mei, A. L. Appleton, D. H. Kim, H. Wang, Z. Bao, *Nat. Commun.* **2013**, 4, 1859.
[15] N. R. Hosseini, J.-S. Lee, *Adv. Funct. Mater.* **2015**, 25, 5586.
[16] M. Amjadi, S. Sheykhansari, B. J. Nelson, M. Sitti, *Adv. Mater.* **2018**, 30, 1704530.
[17] J. Di, S. Yao, Y. Ye, Z. Cui, J. Yu, T. K. Ghosh, Y. Zhu, Z. Gu, *ACS Nano* **2015**, 9, 9407.
[18] W. Honda, S. Harada, T. Arie, S. Akita, K. Takei, *Adv. Funct. Mater.* **2014**, 24, 3299.
[19] X. Wang, Z. Liu, T. Zhang, *Small* **2017**, 13, 1602790.
[20] X. Wang, C. Yan, H. Hu, X. Zhou, R. Guo, X. Liu, Z. Xie, Z. Huang, Z. Zheng, *Chem. - Asian J.* **2014**, 9, 2170.
[21] D. Wang, Y. Zhang, X. Lu, Z. Ma, C. Xie, Z. Zheng, *Chem. Soc. Rev.* **2018**, 47, 4611.

[22] R. Guo, Y. Yu, Z. Xie, X. Liu, X. Zhou, Y. Gao, Z. Liu, F. Zhou, Y. Yang, Z. Zheng, *Adv. Mater.* **2013**, 25, 3343.
[23] S. Liang, Y. Li, T. Zhou, J. Yang, X. Zhou, T. Zhu, J. Huang, J. Zhu, D. Zhu, Y. Liu, C. He, J. Zhang, X. Zhou, *Adv. Sci.* **2017**, 4, 1600313.
[24] Y.-C. Liao, Z.-K. Kao, *ACS Appl. Mater. Interfaces* **2012**, 4, 5109.
[25] F.-T. Zhang, L. Xu, J.-H. Chen, B. Zhao, X.-Z. Fu, R. Sun, Q. Chen, C.-P. Wong, *ACS Appl. Mater. Interfaces* **2018**, 10, 2075.
[26] A. Polywka, T. Jakob, L. Stegers, T. Riedl, P. Görrn, *Adv. Mater.* **2015**, 27, 3755.
[27] M. S. Miller, G. J. E. Davidson, B. J. Sahli, C. M. Mailloux, T. B. Carmichael, *Adv. Mater.* **2008**, 20, 59.
[28] S. Nardecchia, D. Carriazo, M. L. Ferrer, M. C. Gutiérrez, F. del Monte, *Chem. Soc. Rev.* **2013**, 42, 794.
[29] Y. You, Z. Yaokang, L. Kan, Y. Casey, Z. Zijian, *Small* **2015**, 11, 3444.
[30] R. Guo, Y. Yu, J. Zeng, X. Liu, X. Zhou, L. Niu, T. Gao, K. Li, Y. Yang, F. Zhou, *Adv. Sci.* **2015**, 2.
[31] N. Selvakumar, H. C. Barshilia, *Sol. Energy Mater. Sol. Cells* **2012**, 98, 1.
[32] S. J. Limb, K. K. Gleason, D. J. Edell, E. F. Gleason, *J. Vac. Sci. Technol., A* **1997**, 15, 1814.
[33] Y. Sun, J. A. Rogers, *Adv. Mater.* **2007**, 19, 1897.
[34] A. P. Abbott, K. J. McKenzie, *Phys. Chem. Chem. Phys.* **2006**, 8, 4265.
[35] O. Azzaroni, Z. Zheng, Z. Yang, W. T. Huck, *Langmuir* **2006**, 22, 6730.
[36] H. Zhang, P. Zhang, H. Zhang, X. Li, L. Lei, L. Chen, Z. Zheng, Y. Yu, *ACS Appl. Mater. Interfaces* **2018**, 10, 28963.
[37] X. Liu, X. Zhou, Y. Li, Z. Zheng, *Chem. - Asian J.* **2012**, 7, 862.
[38] X. Liu, H. Chang, Y. Li, W. T. Huck, Z. Zheng, *ACS Appl. Mater. Interfaces* **2010**, 2, 529.
[39] C. Zhu, Y. Li, X. Liu, *Polymers* **2018**, 10, 573.
[40] X. Lin, M. Wu, L. Zhang, D. Wang, *ACS Appl. Electron. Mater.* **2019**, 1, 397.
[41] H. Lee, S. M. Dellatore, W. M. Miller, P. B. Messersmith, *science* **2007**, 318, 426.
[42] C. Zhu, X. Guan, X. Wang, Y. Li, E. Chalmers, X. Liu, *Adv. Mater. Interfaces* **2019**, 6, 1801547.
[43] S. M. Burkinshaw, N. Kumar, *Dyes Pigm.* **2009**, 80, 53.
[44] S. Hong, J. Yeom, I. T. Song, S. M. Kang, H. Lee, H. Lee, *Adv. Mater. Interfaces* **2014**, 1, 1400113.
[45] E. Y. Pisarevskaya, V. I. Zolotarevskiy, L. P. Kazanskiy, E. V. Ovsyannikova, N. M. Alpatova, *Synth. Met.* **2009**, 159, 304.
[46] A. S. Mahadevi, G. N. Sastry, *Chem. Rev.* **2013**, 113, 2100.
[47] J. P. Van Buren, W. B. Robinson, *J. Agric. Food. Chem.* **1969**, 17, 772.
[48] X. Wang, H. Hu, Y. Shen, X. Zhou, Z. Zheng, *Adv. Mater.* **2011**, 23, 3090.
[49] J. K. Mason, R. Ehrenborg, E. A. Lazar, *J. Phys. A: Math. Theor.* **2012**, 45, 065001.
[50] S. Hilgenfeldt, A. M. Kraynik, S. A. Koehler, H. A. Stone, *Phys. Rev. Lett.* **2001**, 86, 2685.
[51] I. Hayashi, M. Sato, M. Kuroda, *J. Mech. Phys. Solids* **2011**, 59, 1731.
[52] Y. Mao, M. Zhu, W. Wang, D. Yu, *Soft Matter* **2018**, 14, 1260.
[53] B. Zhang, J. Lei, D. Qi, Z. Liu, Y. Wang, G. Xiao, J. Wu, W. Zhang, F. Huo, X. Chen, *Adv. Funct. Mater.* **2018**, 28, 1801683.
[54] Y.-h. Wu, H.-z. Liu, S. Chen, X.-c. Dong, P.-p. Wang, S.-q. Liu, Y. Lin, Y. Wei, L. Liu, *ACS Appl. Mater. Interfaces* **2017**, 9, 20098.
[55] D. Kang, P. V. Pikhitsa, Y. W. Choi, C. Lee, S. S. Shin, L. Piao, B. Park, K.-Y. Suh, T.-i. Kim, M. Choi, *Nature* **2014**, 516, 222.